PHYSICAL REVIEW B VOLUME 24, NUMBER 8 15 OCTOBER 1981

Polarized-low-energy-electron-diffraction study of the mechanism of electron reflection from W(001) at low energies

E. G. McRae
Bell Laboratories, Murray Hill, New Jersey 07974

D. T. Pierce, G.-C. Wang, and R. J. Celotta
National Bureau of Standards, Washington, D.C. 20234
(Received 11 May 1981)

Polarized-low-energy-electron-diffraction (PLEED) measurements on W(001) are reported for incidence conditions close to the (01) beam threshold [energies $2<E<9$ eV, polar angles $15°<\theta<45°$, (01) azimuth]. The intensity structure $I(E)$ on the low-energy side of the threshold is found to depend on the spin polarization of the incident electrons. For $\theta>25°$, corresponding peaks in $I^{\uparrow}(E)$ and $I^{\downarrow}(E)$ are split in proportion to their width [symbols $\uparrow$ ($\downarrow$) designate spin up (down) with respect to the scattering plane]. For $\theta<25°$ the splitting-to-width ratio increases, and a shoulder grows up on the low-energy side of the lowest-energy peak of $I^{\uparrow}(E)$. The observations are explained by the superposition of reflection-amplitude contributions from "direct" or single scattering at the substrate and "indirect" processes in which the (01) beam is multiply reflected between the substrate and the surface-potential barrier. For $\theta>25°$ the differences between $I^{\uparrow}(E)$ and $I^{\downarrow}(E)$ derive from the spin dependence of the phase of superposition of direct and indirect amplitude terms. The main effects come from the first indirect term, which corresponds to a single reflection at the surface potential barrier. For $\theta<25°$ there are additional important contributions from higher-order indirect terms. These terms add coherently to produce a resonance perturbation of the line shape of $I^{\uparrow}(E)$. The present results, taken together with earlier LEED results, indicate that the threshold interference mechanism is the dominant mechanism of very low-energy (<10 eV) electron reflection at the W(001) surface.

I. INTRODUCTION

Polarized-low-energy-electron-diffraction (PLEED) experiments[1–4] have confirmed predictions[5–7] that the intensity of elastic electron reflection at crystal surfaces should be strongly spin dependent. A potential advantage of PLEED studies is that analysis of the spin dependence might give an improved description of electron reflection mechanisms, especially for incidence energies and angles near threshold (grazing emergence) conditions for diffracted beams.[8] We report PLEED observations and theory for specular reflection from W(001) in the range of low energies where LEED intensities show sharp structure converging on the (01) beam threshold.[9]

Our analysis of the PLEED data correlates spin dependence and the reflection intensity. We show that over the entire energy range up to and slightly beyond the (01) beam threshold, the observations can be accounted for very well by a mechanism related to the grazing emergence of a diffracted beam at its threshold. The intensity structure very close to the threshold has been interpreted in this way, but the origin of the lower-lying structure, in particular the broad peak near 3.5 eV, has been questioned.[10] From our analysis of the PLEED measurements, we conclude that this peak is part of a series converging on the threshold, and that the threshold mechanism is the dominant mechanism of electron reflection from W(001) at low energies.

II. EXPERIMENTS AND RESULTS

The PLEED apparatus and procedure and the preparation of the W(001) surface have been described previously.[4] The temperature of the W crystal was held at 500–600 °C to maintain a (1×1) surface periodicity. The experiment was done with spin-polarized incident electrons and the results were analyzed to determine the specular reflection intensities $I^{\uparrow\downarrow}$ for incident electrons 100%

polarized with spin up (↑) or down (↓) relative to the scattering plane. The measured quantities were the spin-averaged intensity $(I^{\uparrow}+I^{\downarrow})/2$ and the Sherman function $(I^{\uparrow}-I^{\downarrow})/(I^{\uparrow}+I^{\downarrow})$, representing the incident electron-spin dependence of specular reflection intensity. The measurements were made in the (01) azimuth for nominal polar angles of incidence from 15° to 37.5° in 2.5° steps. The absolute error in the measurement of the Sherman function was $\pm 2\%$.

The energy of the electron beam relative to the vacuum level of tungsten was varied by the retarding field method used in earlier studies of the intensity of low-energy-electron reflection at W(001).[11] An applied potential on the W crystal from 12 to 0 V gave incident electron energies E from 0 to 12 eV. Results in the range 2–9 eV are reported. The retarding field at the crystal causes the true angles of incidence to be greater than the nominal angle of incidence by amounts ranging from 1° to 8° in the present experiments. The true angle of incidence θ at the (01) beam threshold was determined from the observed threshold energy $E_{\infty g}$, corresponding to maximum slope of the intensity plot. The formulas used were $E_{\infty g}(\vec{k}_{||})=\frac{1}{2}\,|\,\vec{k}_{||}+2\pi\vec{g}\,|^{2}$ and $k_{||}=(2E)^{1/2}\sin\theta$ (Hartree atomic units). Here $\vec{k}_{||}$ denotes the reduced surface-parallel momentum and $\vec{g}$ denotes the reciprocal-net vector with components (0,1) referred to the basic vectors of the W(001) reciprocal net.

The energy resolution of the PLEED electron source was 0.1 eV. The angle resolution of the source was not measured, but from the widths of intensity structure near threshold it was found that the combined effect of angle and energy resolution was equivalent to an energy resolution of 0.3 eV in the present experiments.

The experimental results are shown in Fig. 1 by plots of $I^{\uparrow}$ and $I^{\downarrow}$ versus energy E. Individually these plots resemble the corresponding intensity plots in LEED—that is, they consist of progressively narrower peaks converging on the (01) beam threshold. As shown in Fig. 1, the difference between $I^{\uparrow}$ and $I^{\downarrow}$ is generally small for energies above the threshold and also for energies far to the low-energy side of the threshold. Other regularities in the results are most conveniently described separately for incidence angles above and below about 25°. For $\theta>25°$, $I^{\uparrow}-I^{\downarrow}$ vanishes close to the intensity extrema, so that the spin dependence can be described as the splitting of each of the two corresponding peaks in $I^{\uparrow}(E)$. For $\theta<25°$ a shoulder grows up on the low-energy side of the lowest-energy peak of $I^{\uparrow}(E)$, and this evolves into a double-peaked structure at low angles (Fig. 1). The peak-shoulder separation has a constant value about 20% less than the width [full width at half maximum (FWHM)] of the lowest-energy peak in $I^{\downarrow}(E)$.

The observed splitting ΔE and widths w of the peaks that are present for all polar angles of incidence are summarized in Fig. 2. For $\theta>25°$, the splitting-to-width ratio $\Delta E/w$ is about the same for both peaks. For θ decreasing below 25°, there is a progressive increase of the peak splitting coinciding with the growth of the low-energy shoulder in $I^{\uparrow}(E)$.

III. THEORY

Our theoretical description is an extension of one derived previously without regard to spin.[10,12] The description neglecting spin yields an expression for the reflection amplitude T and hence the reflection intensity $I=|\,T\,|^{2}$ for a given diffracted beam. A simplified form of the theory is shown schematically in Fig. 3. Figure 3 refers specifically to the (00) beam in the vicinity of the threshold of the $\vec{g}$th diffracted beam. For example, in application to the present experiments $\vec{g}$ designates the (01) beam. The essential element of the description is indirect reflection involving a "preemergent" beam—i.e., a beam whose surface normal momentum is slightly less than that required for grazing emergence. The indirect processes consist of: (1) diffraction into the preemergent beam traveling almost parallel to the surface, (2) multiple scattering of the preemergent beam between the substrate and surface potential barrier, and (3) diffraction from the preemergent to an outgoing propagating beam. In the scheme shown in Fig. 3, symbols S_{gg} and T^{0}_{gg} denote amplitude coefficients of specular reflection of the preemergent beam at the surface potential barrier and substrate, respectively, while T^{0}_{0g} and T^{0}_{g0} denote amplitude coefficients for diffraction into and out of the preemergent beam. Amplitude coefficients of transmission and reflection of the zeroth beam at the surface potential barrier are taken in a simplifying approximation to be 1 and 0, respectively. The surface barrier potential is assumed laterally smooth so that off-diagonal amplitudes such as S_{0g} are negligible. An expression for the reflection amplitude T_{00} that takes account of the indirect processes shown in Fig. 3 is

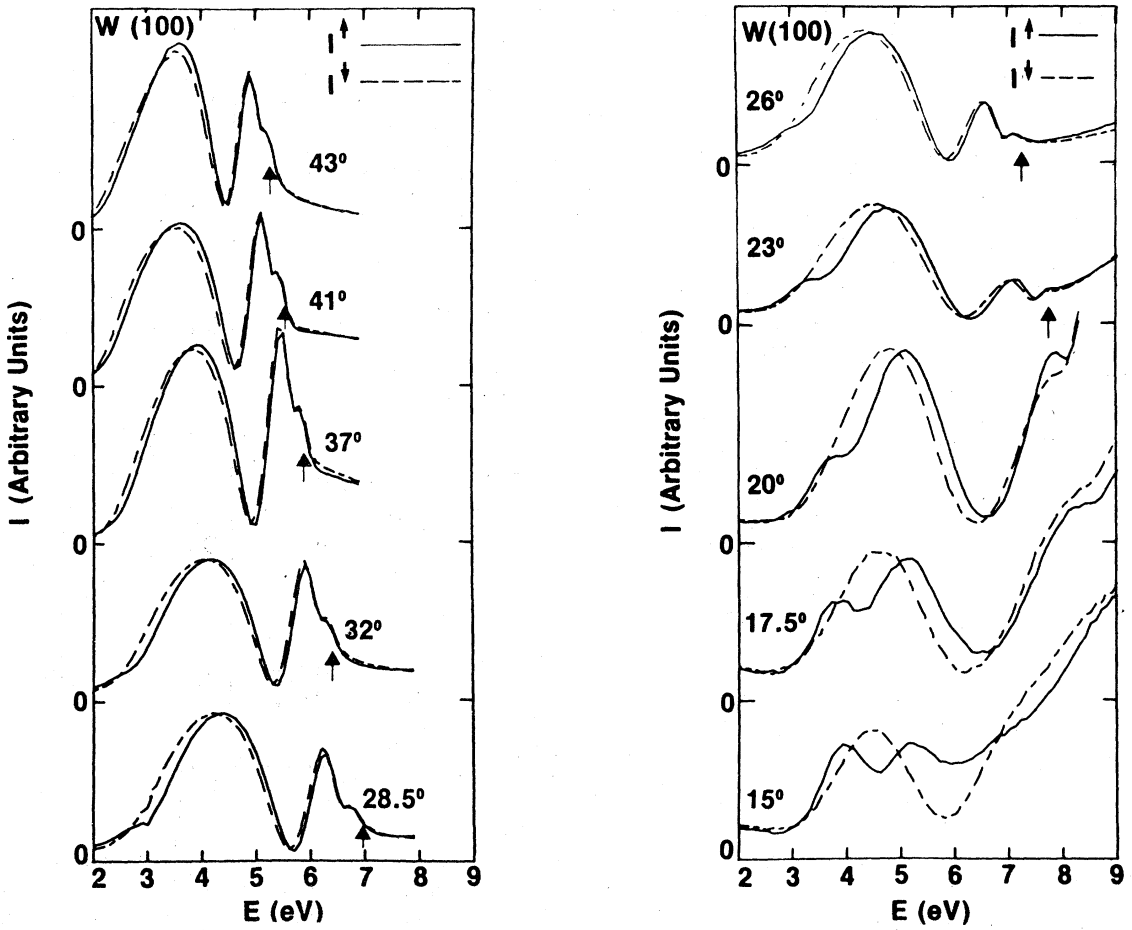

FIG. 1. Specular elastic reflection intensities $I^{\uparrow}$ (solid lines) and $I^{\downarrow}$ (broken lines) plotted against electron energy E. $\uparrow$ ($\downarrow$) denote incident electron spin polarization up (down) with respect to the scattering plane. The measurements were made for the incident beam in the (01) azimuth and for the polar incidence angles indicated. The indicated values of incidence angle are corrected to fit the (01) beam threshold energies estimated from the curves. Representative estimates of threshold energy are indicated by arrows. The 15°, 17.5°, and 20° curves are plotted on a 5× enlarged scale.

$$T_{00}=T_{00}^{0}\left[1+\frac{RS_{gg}}{1-T_{gg}^{0}S_{gg}}\right], \tag{1}$$

where $R\equiv T_{0g}^{0}T_{g0}^{0}/T_{00}^{0}$. The first term in parentheses represents the direct contribution and the second term the indirect contribution to the total amplitude T_{00}. The second- and higher-order indirect amplitude contributions together represent the resonance scattering in which the incident electrons enter temporary surface states. These terms form a geometric series whose summation gives the resonance denominator of the indirect contribution.

In application to LEED for metal surfaces, Eq. (1) explains the intensity structure near beam thresholds as arising essentially from the variation of the phase $\arg S_{gg}$ of the surface barrier reflection amplitude. We express the phase in units of π by writing $\sigma\equiv\pi^{-1}\arg S_{gg}$. Approaching the threshold, the substrate amplitude coefficients vary relatively slowly but σ varies increasingly rapidly as a function of the energy E and reduced parallel momentum $\vec{k}_{||}$ of the incident beam. This rapid phase variation is due to the long-range character of the surface barrier potential. For a barrier potential having the "image" form for large distances from the surface, the phase goes to infinity at the threshold according to[10]

$$\sigma(E,\vec{k}_{||})\propto[E_{\infty g}(\vec{k}_{||})-E]^{-1/2},\quad E<E_{\infty g}\ . \tag{2}$$

On the other hand, the value of $|S_{gg}|$ is slowly varying with respect to $(E,\vec{k}_{||})$ over a range of energy that for a given value of $\vec{k}_{||}$ extends down from the threshold energy by an amount roughly equal to the height ΔU of the long-range part of the surface potential barrier. For energies passing outside this range, $|S_{gg}|$ drops relatively rapidly

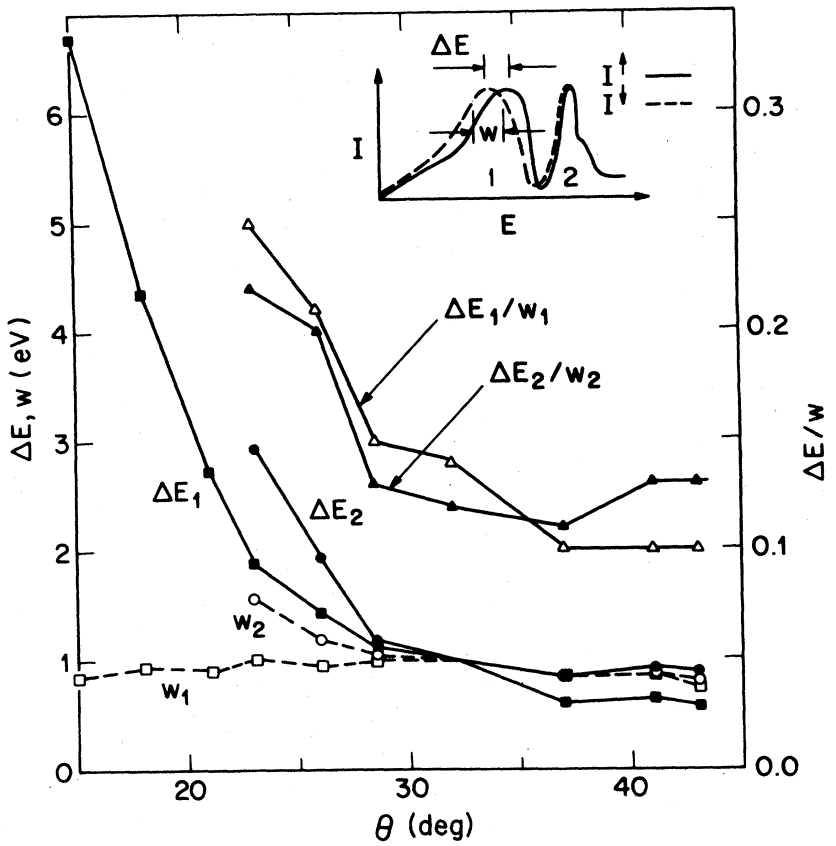

FIG. 2. Summary of observed splittings ΔE and widths w of peaks 1 and 2 in observed $I^{\uparrow\downarrow}(E)$ plots. The peak widths indicated are full widths at 90% maximum height (see inset for notation). The squares and circles are plots of the indicated ΔE and w values multiplied in each case by a scale factor as follows: filled squares, $\Delta E_1(8.62)$; filled circles, $\Delta E_2(39.07)$; open squares, $w_1(1.8)$; open circles, $w_2(4.76)$.

from nearly unity to nearly zero. For the idealized case of a perfectly periodic substrate crystal, a laterally smooth surface potential barrier and no inelastic scattering, $|S_{gg}|$ would be exactly unity in the energy range extending ΔU below threshold (total internal reflection).

Equation (1) can be extended in a very simple way to account for the regularities in spin dependence observed in the present experiments. The spin dependence derives from the spin-orbit interaction that operates on electrons approaching closely to atomic nuclei.[13] To take this into account, each of the reflection amplitudes such as T^0_{0g} must be replaced by the corresponding 2×2 spin scattering matrix.[13] However, the reflection at the surface potential barrier should be independent of spin because it takes place far from the atomic nuclei. Thus S_{gg} should be replaced simply by S_{gg} times the 2×2 unit matrix. We assume that the spin dependence of the numerator of the indirect term is weak, so that terms of second or higher order with respect to the off-diagonal matrix elements can be neglected. With these simplifications, we get in place of Eq. (1)

$$T^{\uparrow\downarrow}_{00}=(T^0_{00}\pm\delta T^0_{00})\left[1+\frac{(R\pm\delta R)S_{gg}}{1-(T^0_{gg}\pm\delta T^0_{gg})S_{gg}}\right], \tag{3}$$

where the upper and lower signs refer to spins ↑ and ↓, respectively. The quantities δT^0_{00}, δR, and δT^0_{gg} represent the spin dependence. Their relationship to the spin scattering matrices is given in Appendix A.

We first apply Eq. (3) to rationalize the regularities observed for incidence angles $\theta>25°$. To reproduce the observations that $I^{\uparrow}-I^{\downarrow}$ is small at energies above threshold (where $|S_{gg}|\approx0$) and at intensity extrema, both $\mathrm{Re}(\delta T^0_{00}/T^0_{00})$ and $\mathrm{Re}(\delta R/R)$ must be negligibly small. The first provision indicates no spin dependence for energies more than the barrier height ΔU below threshold

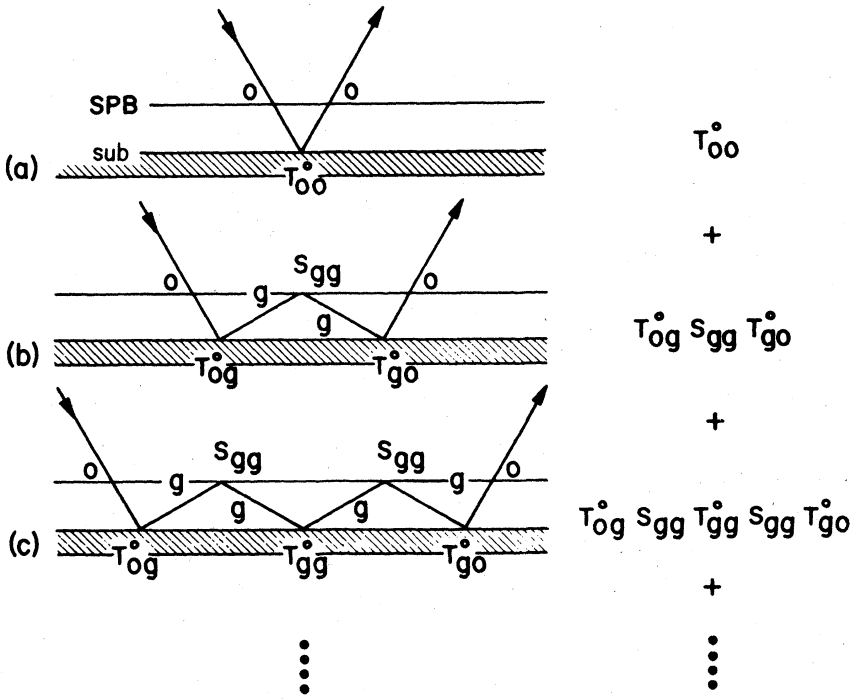

FIG. 3. Schematic indication of direct and indirect reflection processes. Horizontal lines represent the surface potential barrier (SPB) and substrate (sub). The incident and specularly reflected beams are labeled 0. The preemergent beams are labeled g. Symbols T^0 and S denote amplitude coefficients of reflection at the substrate and surface potential barrier, respectively. Panel (a) represents the direct process. Panels (b) and (c) represent the first two indirect processes. Expressions at the right of each panel give the corresponding contribution to the reflection amplitude.

(where again $|S_{gg}| \approx 0$), and this apparently consistent with small $I^{\uparrow} - I^{\downarrow}$ as is observed far below threshold.

The observed regularities for $\theta > 25°$ are well reproduced using approximations and parameter values that have already been found to apply in a detailed treatment of the intensity structure observed in high-resolution LEED for Cu(001).[14] This earlier work is followed by setting $|S_{gg}| = 0$ or 1, by assigning constant values to $|R|$, $\rho \equiv \pi^{-1}\arg R$, and $\delta\rho \equiv \pi^{-1}\mathrm{Im}(\delta R/R)$, and by neglecting the denominator term $(T^0_{gg} \pm \delta T^0_{gg})S_{gg}$. Physically this last provision is equivalent to neglecting the second- and higher-order indirect processes that are responsible for the resonance scattering. The intensity structure is thus attributed entirely to interference between the direct and first indirect amplitude terms [(a) and (b) in Fig. 3]. With these provisions and $|S_{gg}| = 1$, Eq. (3) reduces to[15]

$$T^{\uparrow\downarrow}_{00} \propto 1 + |R| \exp\{i\pi[\rho \pm \delta\rho + \sigma(E)]\} . \quad (4)$$

and the maxima of the intensities $I^{\uparrow\downarrow} = |T^{\uparrow\downarrow}_{00}|^2$ occur at energies given by

$$\rho \pm \delta\rho + \sigma(E) = 2n, \quad n = 1,2,\ldots . \quad (5)$$

The meaning of Eq. (5) is illustrated in Fig. 4(a), where the indicated shape of $\sigma(E)$ is that required to account for the present experiments. This shape is consistent with the existence of the threshold singularity described by Eq. (2). As is evident from Fig. 4(a), for small positive values of $\delta\rho$ we have the expression

$$I^{\uparrow\downarrow}(E) = I(E \mp w(E)\delta\rho) , \quad (6)$$

where I is the intensity obtained from Eq. (4) with $\delta\rho = 0$ and $w(E) \equiv (d\sigma/dE)^{-1}$. Since the intensity peaks occur at equal intervals of $\sigma(E)$, $w(E)$ has the meaning of a moving peak width, i.e., $w(E_{\mathrm{peak}})$ is the width of an intensity peak located at energy E_{peak}. Equation (6) means that the intensities $I^{\uparrow}$ and $I^{\downarrow}$ are the same except for a splitting that is proportional to the peak width and that approaches zero for energies approaching the beam threshold. This is illustrated in Fig. 4(b) by the results of a calculation done in accordance with Eq. (4). In this calculation the value of $|\delta\rho|$ was chosen to reproduce the observed peak splitting.

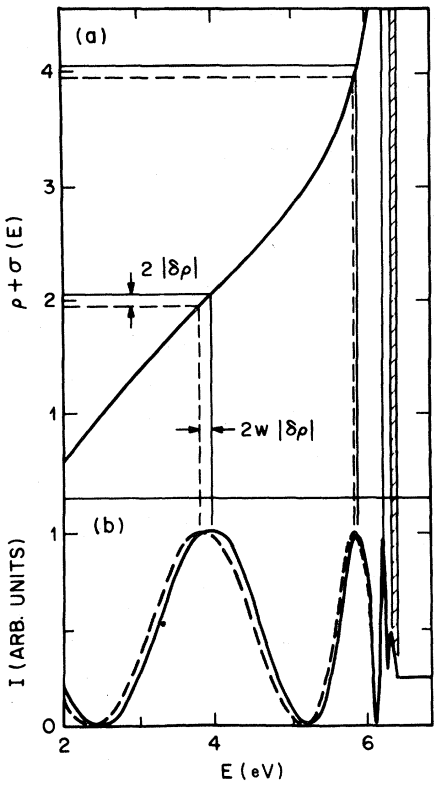

FIG. 4. (a) Plot of the phase $\rho+\sigma(E)$ against energy E (solid line) illustrating the conditions $\rho\pm\delta\rho+\sigma(E)=2n$ given by Eq. (5) (horizontal solid and broken lines) and the energy values at which the conditions are satisfied (vertical solid and broken lines). Each pair of energy values corresponds to a peak of the spin-averaged reflection intensity. The higher and lower members of each pair give the energies of corresponding peaks of $I^{\uparrow}(E)$ and $I^{\downarrow}(E)$, respectively. The splitting of the peaks is proportional to $w\equiv(d\sigma/dE)^{-1}$. The calculation of $\sigma(E)$ was done for polar angle of incidence $\theta=32°$. The value of $|\delta\rho|$ is that required to reproduce the observed peak splittings. (b) Calculated intensity plots illustrating the splitting of spin components as described by Eq. (4): $\theta=32°$. The shaded column indicates energies for which the peak separation is less than the interval between calculated points. Its right-hand edge is the threshold energy.

The smallness of $|\delta\rho|$ justifies the neglect of higher-order terms in the derivation of Eq. (3).

Equation (4) cannot account for the observations for $\theta<25°$. The appearance of a shoulder or double-peaked structure in either polarization can be explained, however, by including the second- and higher-order indirect amplitude terms that describe the resonance scattering. To show this as simply as possible, we add the leading resonance term to the amplitude expression in Eq. (4), omitting explicit indication of the spin. The result is

$$T\propto 1+|R|\exp\{i\pi[\rho+\sigma(E)]\}+|RT_{gg}^{0}|\exp\{i\pi[\rho+\tau+2\sigma(E)]\}\ , \quad (7)$$

where $\tau\equiv\pi^{-1}\arg T_{gg}^{0}$. The effect of the added amplitude term depends on the phase difference $\rho-\tau$. For example, if $\rho-\tau$ is an even integer, the effect is to enhance the intensity peaks that occur at energies satisfying $\rho+\sigma=2n$ [n integer, cf. Eq. (5)], while if $\rho+\sigma=2n+1$ the effect is to depress the intensity at energies satisfying $\rho+\sigma=2n$ and to add intensity at energies satisfying $\rho+\sigma=2n+\frac{1}{2}$ and $\rho+\sigma=2n-\frac{1}{2}$. The centers of added intensity are separated in energy by the width (FWHM) of the peak calculated with $T_{gg}^{0}=0$, but the actual energy separation of the resulting intensity features will be somewhat less than this because of the oppositely sloping backgrounds due to the first two terms of Eq. (7).

The trends observed for $\theta<25$ (Fig. 1) are apparently due to resonance scattering. They would be explained qualitatively by Eq. (7) if the magnitude of $T_{g}^{0\uparrow}\equiv T_{gg}^{0}+\delta T_{gg}^{0}$ increased with decreasing θ while the phase approached the condition $\rho-\tau=2n+1$. Both the appearance of features in $I^{\uparrow}(E)$ separated by slightly less than the width of the corresponding peak in $I^{\downarrow}(E)$ and the enhanced splitting-to-width ratio for $\theta<25°$ (Fig. 2) follow naturally from Eq. (7).

As well as explaining the main regularities in the observations, the theory including indirect processes can also account semiquantitatively for the observed line shapes. This is illustrated in Fig. 5, where some representative line shapes calculated by Eq. (3) are compared with observed ones. The calculations were done with $|S_{gg}|=0$ or 1, $|R|=1$, and fixed values of other parameters as given in Fig. 5 caption. The background intensity $|T_{00}^{0}|^{2}$ was assumed energy independent, and all intensity curves were normalized to the same maximum intensity. The phase $\sigma(E)$ of the surface barrier reflection amplitude was calculated for a barrier potential $U(z)$ that has the image form $-1/[4(z-z_0)]$ (Hartree atomic units) at large distances z from the surface and joins smoothly to a linear potential at smaller distances. The parameters z_0 and $U(0)$ characterizing the potential were assigned numerical values that were earlier found to give a fit using this form of potential to high-resolution LEED data for Cu(001).[14] The values used were $z_0=4$ a.u., $U(0)=-7$ eV. The calculations were done for incidence angles corrected for the deflection due to the retarding potential as

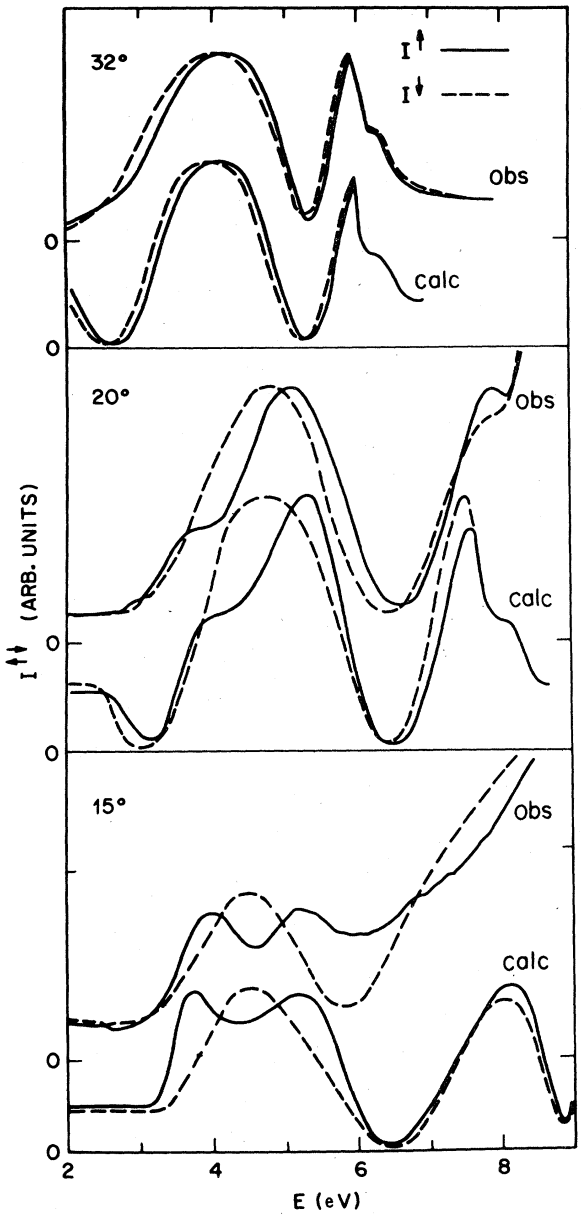

FIG. 5. Comparison of line shapes $I^{\uparrow\downarrow}(E)$ calculated from Eq. (3) (calc) with observed line shapes (obs) for representative polar angles of incidence shown at top left of each panel. The observed line shapes are the same as shown in Fig. 1. The calculations were done with $T_{gg}^{0}-\delta T_{gg}^{0}$ equal to $0.1\exp(i0.275\pi)$ and other parameter values as follows:

$$(\theta,\rho+\delta\rho,\rho-\delta\rho,T_{gg}^{0}+\delta T_{gg}^{0})$$
$$=(32°,1.23,1.30,0.1\exp(i0.275\pi))$$
$$=(21°,1.63,1.70,0.35\exp(i0.728\pi))$$
$$=(15°,0.33,0.33,0.4\exp(i1.23\pi)).$$

The calculated curves were normalized to the same maximum intensity as the observed ones.

described in Appendix B. The intensities calculated from Eq. (3) were convoluted with a Gaussian of FWHM 0.3 eV to simulate the combined effect of incident energy spread and angular divergence.

As illustrated in Fig. 5, the theory reproduces the observed line shapes near the center of the low-energy intensity structure, but there are discrepancies on the low-energy side for all values of θ and there are discrepancies also on the high-energy side for $\theta<25°$. The discrepancies on the low-energy side are probably due to the artificial provision in the calculation that the value of $|S_{gg}|$ drops suddenly from 1 to 0 when the energy displacement from the threshold exceeds the barrier height $\Delta U=-U(0)$. The inclusion of inelastic scattering would cause $|S_{gg}|$ to change more slowly, thereby removing the spurious interference structure near and below 3 eV in the theoretical curves. The discrepancies on the high-energy side may be related to the energy dependence of the background intensity, which experimentally is relatively high for $\theta<25°$ (note that the 15°, 17.5°, and 20° curves in Fig. 1 are plotted on a 5× enlarged scale).

IV. MECHANISM OF ELECTRON REFLECTION AT W(001) SURFACE

The significance of the present PLEED results may be understood in the context of previous LEED results for W(001).[9,11,16,17] The results are summarized in Fig. 6, which maps the energies and $k_{||}$ values for peaks in intensity plots for incidence directions in the (01) azimuth.

The changes of the intensity-energy plots as $k_{||}$ increases may be described as follows.[11] For $k_{||}=0$ there are intensity peaks at 4 and 8 eV. As $k_{||}$ increases, the lowest-energy peak (A in Fig. 6) remains near 4 eV while the other peak C weakens and splits into two components. Subsequently a third peak B appears between 4 and 8 eV.

For normal incidence ($k_{||}=0$) the peaks A and C derive from scattering at the substrate. Both the positions and intensities of these peaks were reproduced well by relativistic LEED calculations of Jennings and Read[18] that did not include scattering at the surface potential barrier. Peak A coincides with a narrow absolute band gap in the relativistic band structure as calculated and checked experimentally by Willis and Christensen.[19] The gap edges in the section of reciprocal space relevant to the present discussion are reproduced in Fig. 6. Jennings and Read[18] suggested that peak A derives from a particular feature of scattering by W atoms,

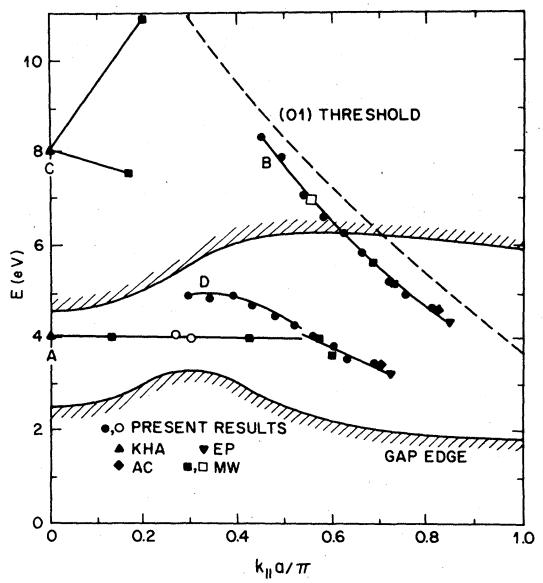

FIG. 6. Positions of elastic electron reflection (00) intensity peaks and related data for W(001) surface. The results refer to reduced parallel momentum $k_{||}$ in the (01) direction. Energies E of intensity peaks (points) gap edges (shaded lines), and the (01) threshold (broken line) are plotted against $k_{||}a/\pi$ where a is the W(001) net side (3.16 Å). Full lines drawn through points indicate major trends in peak positions. Letters identify peaks or groups of peaks discussed in the text. Circles indicate positions of peaks (filled circles) or shoulders (open circles) from the present work. Other symbols indicate positions of peaks (filled symbols) or shoulders (open symbols) from earlier work of Khan, Hobson, and Armstrong (KHA, Ref. 16), Edwards and Propst (EP, Ref. 17), Adnot and Carette (AC, Ref. 9), and McRae and Wheatley (MW, Ref. 11). The positions of the gap edges are as given by Willis and Christensen (Ref. 19).

namely, a sudden rise of the d-wave phase shift for energies increasing just above vacuum level. The dispersionless character of the band gap as calculated by Willis and Christensen[19] is what would be expected if the band gap were due to an atomic scattering property. However, the rise of the d-wave phase shift occurs 2—3 eV below the gap and so could not be directly responsible for it. Peak B was early assigned to structure associated with the (01) threshold,[11,12] and this assignment was subsequently sustained by high resolution LEED results showing that B is a member of a sequence of peaks converging on the threshold.[9,10]

The present observations show peaks or shoulders belonging to the branches A and B (Fig. 6) together with a new branch D that merges into branch A for values of $k_{||}a/\pi$ greater than 0.5. It appears that the peaks observed between 3 and 4 eV are an extension of the branch D. In a discussion of the origin of these peaks[10] it was pointed out that they might fit into a sequence including B that converges on the (01) threshold, but no conclusive assignment could be made on the basis of intensity data alone. *The present measurements of spin dependence as well as intensity show conclusively that the peaks D arise from indirect scattering processes and thus belong to a sequence converging on the (01) threshold.* The observation for $k_{||}a/\pi > 0.4$ ($\theta > 25°$) of a splitting-to-width ratio that is independent of $k_{||}$ and is the same for peaks D and B is an unequivocal sign of an indirect mechanism. The perturbation of peak D associated with the growth of the shoulder A for $k_{||} < 0.4$ is in accord with this interpretation, but the nature of the perturbation would have been difficult to understand from intensity data alone. The measurements of spin dependence as well as intensity clearly show the role of indirect scattering, including especially the resonance scattering.

Further experiments are needed to show the correlation between the normal-incidence ($k_{||}=0$) intensity structure and the structure observed in the angle range of the present experiments. In particular, the splitting of the peak C is not understood. One possibility that could be checked is that the lower-energy split component is a continuation of the branch D. Other unanswered questions concern the values of the parameters that describe the spin dependence through Eq. (3). The qualitative results depend on both $\delta T_{00}^{0}/T_{00}^{0}$ and $\delta R/R$ being imaginary, but no theoretical reason for this is apparent.

We conclude that the peaks B and D all derive from interferences between direct and indirect reflection processes associated with the (01) beam threshold. A similar interpretation might apply to the lower-energy peaks split off from peak C as well. As these peaks are all intense, it follows that the threshold interference mechanism is the dominant mechanism of very low energy (< 10 eV) electron reflection at W(001) surface.

Our findings differ from the conventional physical picture of LEED. According to LEED theory that has been applied successfully for energies above about 20 eV,[20] the elastic electron reflection goes by the direct process [Fig. 3(a)]. Thus the reflection intensity is viewed as arising essentially from ion-core scattering and the associated band gaps (Bragg reflection conditions) of the substrate

crystal. This conventional picture is correct as long as the inelastic electron-electron scattering is strong enough to discriminate overwhelmingly against indirect processes [Figs. 3(b), 3(c), etc.] where there are two or more reflections from the substrate. But in the present instance, where the interference between the direct and indirect processes is the dominant source of intensity, the intensity peaks are related to the beam threshold and not to the band gaps. Our conclusions depend on the ability to measure the spin dependence of electron reflection intensities, and so demonstrate that this extra experimental input can lead to a better description of the reflection mechanism.

ACKNOWLEDGMENT

The part of this work done at the National Bureau of Standards was supported in part by the Office of Naval Research. We are grateful for helpful discussions with J. Rundgren, B. I. Dunlap, and R. E. Dietz.

APPENDIX A: SPIN DEPENDENCE OF REFLECTION AMPLITUDES

Following standard treatments of electron scattering including spin,[13] we represent the incident electron spin by the vectors $2^{-1/2}\binom{1}{\pm 1}$ where the upper and lower signs refer, respectively, to spin up and down with respect to the scattering plane. We replace the reflection amplitude T_{00} by the 2×2 spin scattering matrix $[T_{00}(i,j)]$. The reflection intensity is given by

$$I^{\uparrow\downarrow}=\tfrac{1}{2}[\,|\,T_{00}(11)\pm T_{00}(12)\,|^2 + |\,T_{00}(22)\pm T_{00}(21)\,|^2]\,. \quad \text{(A1)}$$

We consider cases in which the matrix elements have the symmetry

$$T_{00}(11)=T_{00}(22),\quad T_{00}(12)=T_{00}(21)\,, \quad \text{(A2)}$$

so that the intensity is given by $I^{\uparrow\downarrow}=|\,T_{00}^{\uparrow\downarrow}\,|^2$ where

$$T_{00}^{\uparrow\downarrow}=T_{00}(11)\pm T_{00}(12)\,. \quad \text{(A3)}$$

The symmetry Eq. (A2) applies for scattering by isolated atoms and hence for any single-scattering (kinematical) approximation to reflection by a crystal. This symmetry applies because the matrix elements refer to scattering of electrons whose spin polarization is in the plane of scattering. In multiple-scattering (dynamical) approximations there will be, in general, a breakdown of the symmetry because of intermediate scattering out of the plane of incident and reflected beams. However, for incidence in a mirror plane of symmetry of the crystal, the intermediate scattering paths occur in pairs related by mirror symmetry, so that the symmetry Eq. (A2) is retained.

To obtain an expression for the amplitude $T_{00}(11)\pm T_{00}(12)$ we replace the reflection amplitudes in Eq. (1) by 2×2 matrices as follows: $T_{pq}^0\rightarrow[T_{pq}^0(i,j)]$ $(p,q=0,g)$ and $S_{gg}\rightarrow S_{gg}I$ where I is the unit matrix. On carrying out the indicated matrix inversion and multiplications, we get Eq. (3) with the following identifications:

$$\delta T_{pq}^0=T_{pq}^0(12)\,, \quad \text{(A4)}$$

$$\delta R=[T_{0g}^0(11)T_{g0}^0(12) + T_{0g}^0(12)T_{g0}^0(11)]/T_{00}^0(11)+\ldots\,, \quad \text{(A5)}$$

where the ellipsis indicates higher-order terms. "Higher-order terms" refer to terms of second or higher order with respect to off-diagonal matrix elements $T_{pq}^0(12)$.

APPENDIX B: CORRECTION TO INCIDENCE ANGLES FOR RETARDING POTENTIAL DEFLECTION

The model used to calculate the angle correction is shown in Fig. 7. The electrostatic potential V in front of the crystal is assumed to vary linearly with distance from the grid in the space between the grid and the reference plane [Fig. 7(a)], and V is assumed to vary linearly with the polar angle coordinate α between the reference plane and the crystal [Fig. 7(b)]. It is assumed that the potential V_3 at the reference plane is related to the potentials V_2 and V_4 at the grid and crystal, respectively, by

$$V_3=V_4+(V_2-V_4)X\tan\theta_n/D\,, \quad \text{(B1)}$$

where θ_n denotes the nominal polar angle of incidence, D denotes the distance from the crystal to the grid, and X is a distance parameter to be adjusted to fit the observed polar angle of incidence at a beam threshold. The electron energy E is given by $E=V_4-V_1$ where V_1 is the cathode potential.

To calculate the angle of incidence θ for the above model, the equations of motion of the electron between the reference plane and the crystal,

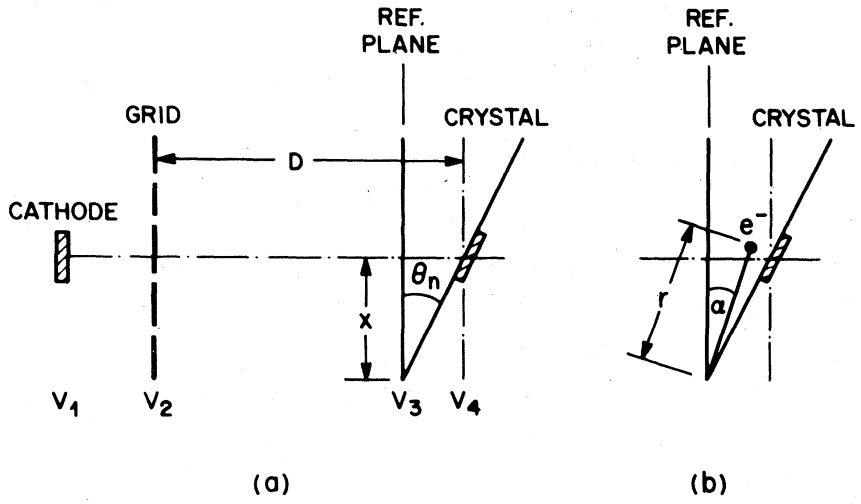

FIG. 7. Model and notations used in calculation of incidence angle correction. (a) Model for the electrostatic potential. (b) Coordinates of electron e^-.

$$\frac{dr}{d\alpha}=r\dot{\alpha}\,, \tag{B2}$$

$$\frac{d(r\dot{\alpha})}{d\alpha}=\frac{V_4-V_3}{\theta_n r\dot{\alpha}}-\dot{r}\,, \tag{B3}$$

were solved numerically for initial conditions

$$r=X,\quad \alpha=0\,, \tag{B4}$$

$$\dot{r}=0,\quad r\dot{\alpha}=[2(V_3-V_1)]^{1/2} \tag{B5}$$

(Hartree atomic units) to determine θ from

$$\tan\theta=\frac{\dot{r}}{r\dot{\alpha}}\bigg|_{\alpha=\theta_n}. \tag{B6}$$

A test of the validity of the model is that the value of X required to fit the observed incidence angles at the threshold energy should be independent of the nominal incidence angle θ_n. In practice the required values lay in the range $0.5D-1.0D$ and did not show any systematic dependence on θ_n. The scatter of values probably reflects the uncertainty in locating the threshold energy. An idea of the size of the angle correction is provided by the following figures: $E=2$ eV, $\theta_n=30°$, $\theta=45°$.

[1]M. R. O'Neill, M. Kalisvaart, F. B. Dunning, and G. K. Walters, Phys. Rev. Lett. 34, 1167 (1975).
[2]R. Feder, N. Müller, and D. Wolff, Z. Phys. B 28, 265 (1977).
[3]J. Kirschner and R. Feder, Phys. Rev. Lett. 42, 862 (1979).
[4]G. -C. Wang, B. I. Dunlap, R. J. Celotta, and D. T. Pierce, Phys. Rev. Lett. 42, 1349 (1979); D. T. Pierce, R. J. Celotta, G. -C. Wang, and E. G. McRae (unpublished).
[5]P. J. Jennings, Surf. Sci. 26, 509 (1971).
[6]R. Feder, Phys. Rev. Lett. 36, 598 (1976).
[7]R. Feder, P. J. Jennings, and R. O. Jones, Surf. Sci. 61, 307 (1976).
[8]P. J. Jennings and R. O. Jones, Surf. Sci. 71, 101 (1977).
[9]A. Adnot and J. D. Carette, Phys. Rev. Lett. 38, 1084 (1977).
[10]E. G. McRae, Rev. Mod. Phys. 51, 541 (1979).
[11]E. G. McRae and G. H. Wheatley, Surf. Sci. 29, 342 (1972).
[12]E. G. McRae, Surf. Sci. 25, 491 (1971).
[13]J. Kessler, *Polarized Electrons* (Springer, Berlin, 1976).
[14]R. E. Dietz, E. G. McRae, and R. L. Campbell, Phys. Rev. Lett. 45, 1280 (1980).
[15]The phase σ is a function of both E and $\vec{k}_{||}$ but for brevity in the following expressions only the E dependence is indicated.
[16]L. H. Khan, J. P. Hobson, and R. A. Armstrong, Phys. Rev. 129, 1513 (1963).
[17]D. Edwards and F. M. Propst, J. Chem. Phys. 56, 3184 (1972).
[18]P. J. Jennings and M. N. Read, J. Phys. C 8, L285 (1975).
[19]R. F. Willis and N. E. Christensen, Phys. Rev. B 18, 5140 (1978).
[20]J. B. Pendry, *Low Energy Electron Diffraction* (Academic, New York, 1974).